

Projected land photosynthesis constrained by changes in the seasonal cycle of atmospheric CO₂

Sabrina Wenzel¹, Peter M. Cox², Veronika Eyring¹ & Pierre Friedlingstein²

Uncertainties in the response of vegetation to rising atmospheric CO₂ concentrations^{1,2} contribute to the large spread in projections of future climate change^{3,4}. Climate–carbon cycle models generally agree that elevated atmospheric CO₂ concentrations will enhance terrestrial gross primary productivity (GPP). However, the magnitude of this CO₂ fertilization effect varies from a 20 per cent to a 60 per cent increase in GPP for a doubling of atmospheric CO₂ concentrations in model studies^{5–7}. Here we demonstrate emergent constraints^{8–11} on large-scale CO₂ fertilization using observed changes in the amplitude of the atmospheric CO₂ seasonal cycle that are thought to be the result of increasing terrestrial GPP^{12–14}. Our comparison of atmospheric CO₂ measurements from Point Barrow in Alaska and Cape Kumukahi in Hawaii with historical simulations of the latest climate–carbon cycle models demonstrates that the increase in the amplitude of the CO₂ seasonal cycle at both measurement sites is consistent with increasing annual mean GPP, driven in part by climate warming, but with differences in CO₂ fertilization controlling the spread among the model trends. As a result, the relationship between the amplitude of the CO₂ seasonal cycle and the magnitude of CO₂ fertilization of GPP is almost linear across the entire ensemble of models. When combined with the observed trends in the seasonal CO₂ amplitude, these relationships lead to consistent emergent constraints on the CO₂ fertilization of GPP. Overall, we estimate a GPP increase of 37 ± 9 per cent for high-latitude ecosystems and 32 ± 9 per cent for extratropical ecosystems under a doubling of atmospheric CO₂ concentrations on the basis of the Point Barrow and Cape Kumukahi records, respectively.

The aim of this study is to reduce the uncertainty in projected large-scale GPP increases, on the basis of the observed trends in the CO₂ amplitude at two measuring sites by applying an emergent constraint^{8–11}. This method utilizes common relationships between observables, such as the CO₂ seasonal cycle, and Earth system sensitivities, such as the CO₂ fertilization of the terrestrial carbon sink, considering the full range of responses from an ensemble of complex Earth system models (ESMs).

It has been hypothesized that increasing GPP has been responsible for an observed increase in the amplitude of the CO₂ seasonal cycle at Mauna Loa, Hawaii¹⁴, but the sensitivity of the seasonal cycle at this high-altitude site to variations in atmospheric circulation has prevented confirmation of this theory¹⁵. Some recent studies also suggest that variations in the Mauna Loa seasonal cycle are partly due to changing agriculture^{12,13}. Here we instead analyse the observed changes in the amplitude of the CO₂ seasonal cycle at Point Barrow, Alaska, a high-latitude station much less affected by mid-latitude agriculture, and at Cape Kumukahi, which is close to Mauna Loa but consists of ground-based measurements that are more directly comparable to the model outputs.

Between 1974 and 2013 the global mean atmospheric CO₂ concentration increased by about 75 p.p.m. by volume (p.p.m.v.) and therefore by about the same amount at Point Barrow (BRW: 71.3° N, 156.6° W),

Alaska, and at Cape Kumukahi (KMK: 19.5° N, 155.6° W), Hawaii, (Extended Data Fig. 1). On top of this increasing CO₂ trend, the uptake and release of carbon by the terrestrial biosphere throughout the year causes a seasonal cycle of CO₂: high concentrations occur in the Northern Hemisphere winter when there is a net release of CO₂ from the land due to the decomposition of organic matter in the soil, and lower values are observed in summer when Northern Hemisphere photosynthesis results in a drawdown of CO₂ (ref. 16). A change in the rate of photosynthesis (for example, due to CO₂ fertilization) or decomposition (due to temperature variability, for instance) will therefore change the amplitude of CO₂ as measured in the atmosphere. In addition, changes in the phase lag between photosynthesis and decomposition, due to the effects of summer drying on photosynthesis or the effects of autumn warming on decomposition¹⁷, can also change the amplitude of the CO₂ seasonal cycle.

The observed CO₂ amplitude at BRW increased from about 13 p.p.m.v. to 18 p.p.m.v. over the available observational record from 1974 to 2013, and from about 8 p.p.m.v. to 9 p.p.m.v. over the length of

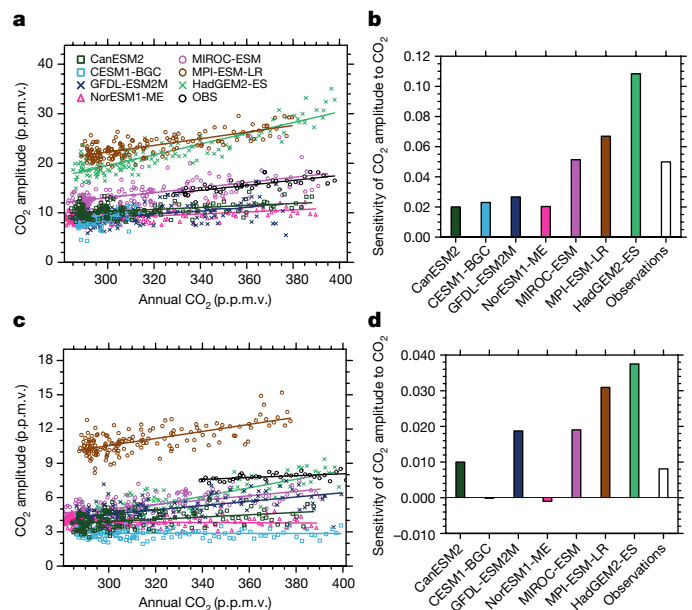


Figure 1 | Comparison of CO₂ seasonal amplitudes for CMIP5 historical simulations and observations. **a, c**, Annual mean atmospheric CO₂ versus the amplitudes of the CO₂ seasonal cycle at BRW (**a**) and KMK (**c**) for observations (black) and CMIP5 historical simulations (colours). Markers show the values for the individual years and the lines show the linear best fit for each model and for the observations. **b, d**, Histogram showing the corresponding gradient of the linear correlations for BRW (**b**) and KMK (**d**). Linear trends are derived for the period 1860–2005 from historical simulations for the models, for 1974–2013 for the BRW observations and for 1979–2015 for the KMK observations.

¹Deutsches Zentrum für Luft- und Raumfahrt (DLR), Institut für Physik der Atmosphäre, Oberpfaffenhofen, Germany. ²College of Engineering, Mathematics & Physical Sciences, University of Exeter, Exeter EX4 4QE, UK.

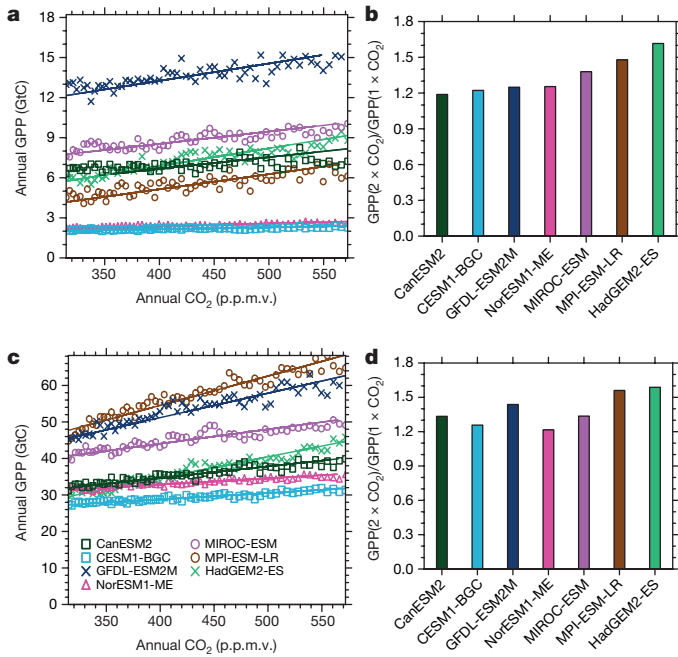


Figure 2 | Comparison of simulated annual mean GPP at a doubling of CO₂ in the 1%BGC simulations. **a, c,** Annual global mean CO₂ increase versus the annual mean GPP in the CMIP5 1%BGC simulations for high-latitude (60° N–90° N) GPP (**a**) and extratropical (30° N–90° N) GPP (**c**). Markers show the values for the individual years and lines show the linear best fit for each model. **b, d,** Histogram showing the relative change in the high-latitude (**b**) and extratropical (**d**) GPP due to a doubling of atmospheric CO₂ (see Methods).

the KMK record (1979–present). To understand and interpret these changes, we make a comparison to ESM simulations that are available via the Coupled Model Intercomparison Project Phase 5 (CMIP5)¹⁸. We analyse seven ESMs that provided outputs from both a fully coupled historical simulation forced with anthropogenic CO₂ emissions for the period 1850–2005 and a biogeochemically (BGC) coupled simulation that excludes climate change effects and has a prescribed atmospheric CO₂ concentration starting from a preindustrial value for 1850 of around 285 p.p.m.v. and then increasing at 1% per year until quadrupling (hereafter referred to as 1%BGC). The comparison between the historical and 1%BGC runs provides information on the relative influence of CO₂ fertilization and climate change on GPP.

Figure 1a, c compares the observed change in the amplitude of the seasonal CO₂ cycle (black markers) to that simulated by each of the seven CMIP5 models in their historical simulations. For consistency with our subsequent analysis, we have plotted the CO₂ amplitude against the annual mean CO₂ at BRW and KMK. The models simulate the CO₂ amplitudes under the present-day CO₂ concentration (approximately 400 p.p.m.v.) over a range of 12–30 p.p.m.v. at BRW (Fig. 1a) and 3–13 p.p.m.v. at KMK (Fig. 1c). Most models simulate an increase in the CO₂ amplitude over time, but the magnitude of this increase varies considerably from model to model, as shown by the linear regression lines in Fig. 1a, c.

Figure 1b, d compares the gradient of these linear regression lines. The observations (black bar) suggest an increase in the CO₂ amplitude of about 0.05 p.p.m.v. per 1 p.p.m.v. increase in annual mean CO₂ at BRW and 0.008 p.p.m.v. per 1 p.p.m.v. at KMK. The models show a large range in this gradient of about 0.02–0.11 p.p.m.v. per 1 p.p.m.v. at BRW and 0–0.04 p.p.m.v. per 1 p.p.m.v. at KMK. Models with major high-latitude vegetation greening (for example, HadGEM2-ES) give large increases in the CO₂ amplitude, whereas models with strong nitrogen limitations on plant growth (CESM1-BGC, NorESM1-ME)

typically show weaker or even slightly negative trends (Fig. 1d). Overall, weaker trends of around 0.02 p.p.m.v. per 1 p.p.m.v. are favoured by four out of the seven CMIP5 models at BRW (Fig. 1b).

The CO₂ amplitude at BRW is well correlated with annual mean high-latitude GPP in each model, indicating that the dominant cause of the increasing amplitude is increasing GPP (Extended Data Fig. 2). The CMIP5 models agree reasonably well on the gradient of this relationship (0.13–0.22 GtC yr⁻¹ per p.p.m.v.), which suggests that the observed increase of 5 p.p.m.v. in the CO₂ amplitude at BRW is consistent with an increase of 0.65–1.1 GtC yr⁻¹ in high-latitude GPP from 1974 to 2013. Changes in the annual mean GPP in the 1%BGC simulations show a slightly smaller rate of increase with CO₂, implying that high-latitude warming is adding to the increase in CO₂ amplitude that is simulated in the historical runs (Extended Data Fig. 3). However, the simulated overall increase in the CO₂ amplitude due to both climate change and CO₂ increase (in the historical simulations) is nearly proportional to that due to CO₂ fertilization alone (from the 1%BGC runs), as shown by the best-fit straight line in Extended Data Fig. 3. As a result, the simulated increase in the CO₂ amplitude remains strongly correlated with the strength of the CO₂ fertilization across the model ensemble. This opens up the possibility of an emergent constraint^{8–11} on CO₂ fertilization.

Figure 2 shows the extent of CO₂ fertilization in these same models at the time of doubling of CO₂ in the 1%BGC runs. The fractional increase in high-latitude (60° N–90° N) GPP due to the doubling of the CO₂ concentrations in these models varies from 20% to 60%, with four of the seven models giving values of less than 25% (Fig. 2b). There is a clear similarity to the histograms showing the sensitivity of the CO₂ amplitude at BRW and KMK to CO₂ (Fig. 1b, d).

The linear relationship between the CO₂ fertilization effect on the CO₂ amplitude at BRW and the relative GPP increase at the time of CO₂ doubling for the CMIP5 models is shown in Fig. 3a, with a correlation coefficient of $r = 0.98$ ($P = 0.0005$; for KMK $r = 0.96$, $P = 0.0004$). Models that simulate a large trend in the CO₂ amplitude at BRW also predict a large high-latitude GPP increase in the future. The combination of the observed trend in the CO₂ amplitude and this model-based linear relationship creates an emergent constraint^{8–11} on the magnitude of CO₂ fertilization of large-scale high-latitude ecosystems in the real world. In the absence of this constraint, the prior probability density function (PDF) for the CMIP5 model spread is shown as the black histogram in Fig. 3b, implying a modal CO₂ fertilization effect of a 20%–25% increase in GPP due to a doubling of CO₂ at BRW. The observed range of the CO₂ fertilization effect at BRW allows a conditional PDF to be calculated by convolving the probability contours around the best-fit straight line in Fig. 3a with the uncertainty in the observed changes of the BRW CO₂ amplitude to annual mean CO₂ concentration^{10,11}. This emergent constraint implies a reduced range of uncertainty for the CO₂ fertilization effect for high-latitude land, with a central estimate of $37\% \pm 9\%$ that is also higher than those suggested by the unweighted CMIP5 models.

We use the same method for the KMK data–model comparison (Fig. 3c, d), but in this case we compare the CO₂ amplitude at KMK with the mean GPP in the entire extratropical Northern Hemisphere (30° N–90° N). We again find that the sensitivity of the CO₂ amplitude to the annual mean CO₂ has an approximately linear relationship with the magnitude of the CO₂ fertilization of GPP (Fig. 3c). This provides an emergent constraint on the CO₂ fertilization of extratropical GPP of $32\% \pm 9\%$ due to doubling CO₂, which overlaps with the estimate of CO₂ fertilization that we derived for BRW ($37\% \pm 9\%$), providing further evidence of robust constraints.

For comparison, the Free Air CO₂ Enrichment (FACE) experiments suggest an increase in net primary productivity of about 23% when averaged across four sites with approximately 1.5 times the pre-industrial CO₂ concentration¹, which is about 0.16% per p.p.m.v. Our larger-scale constraint therefore implies a similar central estimate of CO₂ fertilization on large scales and in the future, (approximately

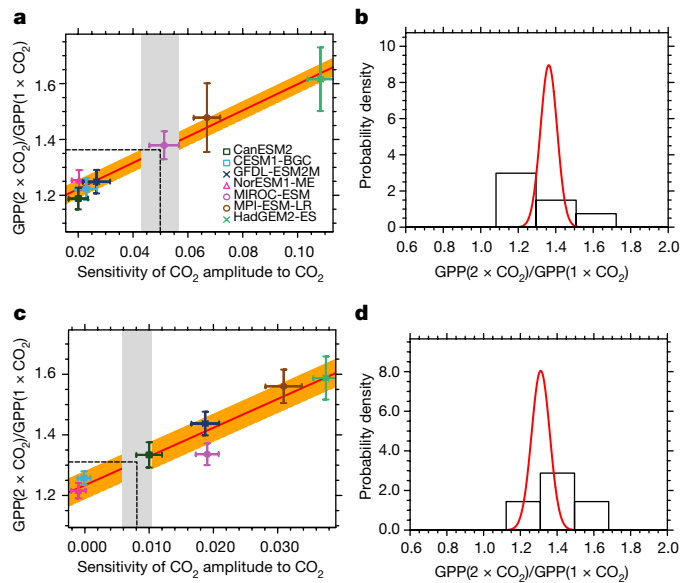


Figure 3 | Emergent constraints on the relative increase of large-scale GPP for a doubling of CO₂. **a, c,** Correlations between the sensitivity of the CO₂ amplitude to annual mean CO₂ increases at BRW (*x* axis) and the high-latitude (60° N–90° N) CO₂ fertilization on GPP at 2 × CO₂ (**a**) and the same for KMK and extratropical (30° N–90° N) GPP (**c**). The grey shading shows the range of the observed sensitivity. The red line shows the linear best fit across the CMIP5 ensemble together with the prediction error (orange) and error bars show the standard deviation for each data point. **b, d,** The probability density histogram for the unconstrained CO₂ fertilization of GPP (black) and the conditional PDF arising from the emergent constraints (red) for BRW (**b**) and KMK (**d**).

0.13% ± 0.03% per p.p.m.v. for high latitudes and 0.11% ± 0.03% per p.p.m.v. for the extratropics), but with significantly reduced uncertainties. Models without nitrogen limitations span the full range of CO₂ fertilization (20%–60%), whereas the current models that include nitrogen limitations appear to underestimate CO₂ fertilization (20%–25%), especially for the extratropical domain. These emergent constraints therefore give a consistent picture of a substantial CO₂-fertilization effect and point to the need for further improvements in the treatment of nutrient limitations in ESMs.

Online Content Methods, along with any additional Extended Data display items and Source Data, are available in the online version of the paper; references unique to these sections appear only in the online paper.

Received 15 June 2015; accepted 8 August 2016.

Published online 28 September 2016.

- Norby, R. J. *et al.* Forest response to elevated CO₂ is conserved across a broad range of productivity. *Proc. Natl Acad. Sci. USA* **102**, 18052–18056 (2005).
- Leakey, A. D. B. *et al.* Elevated CO₂ effects on plant carbon, nitrogen, and water relations: six important lessons from FACE. *J. Exp. Bot.* **60**, 2859–2876 (2009).

- Friedlingstein, P. *et al.* Climate–carbon cycle feedback analysis: results from the C4MIP model intercomparison. *J. Clim.* **19**, 3337–3353 (2006).
- Ciais, P. *et al.* in *Climate Change 2013: the Physical Science Basis* (eds Stocker, T. F. *et al.*) 465–570 (IPCC, Cambridge Univ. Press, 2013).
- Anav, A. *et al.* Evaluating the land and ocean components of the global carbon cycle in the CMIP5 earth system models. *J. Clim.* **26**, 6801–6843 (2013).
- Piao, S. *et al.* Evaluation of terrestrial carbon cycle models for their response to climate variability and to CO₂ trends. *Glob. Chang. Biol.* **19**, 2117–2132 (2013).
- Friedlingstein, P. *et al.* Uncertainties in CMIP5 climate projections due to carbon cycle feedbacks. *J. Clim.* **27**, 511–526 (2014).
- Allen, M. R. & Ingram, W. J. Constraints on future changes in climate and the hydrologic cycle. *Nature* **419**, 224–232 (2002).
- Hall, A. & Qu, X. Using the current seasonal cycle to constrain snow albedo feedback in future climate change. *Geophys. Res. Lett.* **33**, L03502 (2006).
- Cox, P. M. *et al.* Sensitivity of tropical carbon to climate change constrained by carbon dioxide variability. *Nature* **494**, 341–344 (2013).
- Wenzel, S., Cox, P. M., Eyring, V. & Friedlingstein, P. Emergent constraints on climate-carbon cycle feedbacks in the CMIP5 Earth system models. *J. Geophys. Res. Biogeosci.* **119**, 794–807 (2014).
- Keeling, C. D., Chin, J. F. S. & Whorf, T. P. Increased activity of northern vegetation inferred from atmospheric CO₂ measurements. *Nature* **382**, 146–149 (1996).
- Zhao, F. & Zeng, N. Continued increase in atmospheric CO₂ seasonal amplitude in the 21st century projected by the CMIP5 Earth system models. *Earth Syst. Dynam.* **5**, 423–439 (2014).
- Gray, J. M. *et al.* Direct human influence on atmospheric CO₂ seasonality from increased cropland productivity. *Nature* **515**, 398–401 (2014).
- Graven, H. D. *et al.* Enhanced seasonal exchange of CO₂ by northern ecosystems since 1960. *Science* **341**, 1085–1089 (2013).
- Keeling, C., Whorf, T., Wahlen, M. & Plicht, J. Interannual extremes in the rate of rise of atmospheric carbon dioxide since 1980. *Nature* **375**, 666–670 (1995).
- Piao, S. *et al.* Net carbon dioxide losses of northern ecosystems in response to autumn warming. *Nature* **451**, 49–52 (2008).
- Taylor, K. E., Stouffer, R. J. & Meehl, G. A. An overview of CMIP5 and the experiment design. *Bull. Am. Meteorol. Soc.* **93**, 485–498 (2012).

Acknowledgements This work was funded by the Horizon 2020 European Union’s Framework Programme for Research and Innovation under Grant Agreement No. 641816, the Coordinated Research in Earth Systems and Climate: Experiments, Knowledge, Dissemination and Outreach (CRESCENDO) project and the DLR Klimarelevanz von atmosphärischen Spurengasen, Aerosolen und Wolken: Auf dem Weg zu EarthCARE und MERLIN (KiiSAW) project. We acknowledge the World Climate Research Programme (WCRP) Working Group on Coupled Modelling (WGCM), which is responsible for CMIP, and we thank the climate modelling groups for producing and making available their model output. For CMIP the US Department of Energy’s Program for Climate Model Diagnosis and Intercomparison provides coordinating support and led the development of software infrastructure in partnership with the Global Organization for Earth System Science Portals. We thank ETH Zurich for help in accessing data from the ESGF archive.

Author Contributions S.W. led the study and analysis and drafted the manuscript with support from P.M.C. V.E. and P.F. contributed to the concept of the paper and the interpretation of the results. All co-authors commented on and provided edits to the original manuscript.

Author Information Reprints and permissions information is available at www.nature.com/reprints. The authors declare no competing financial interests. Readers are welcome to comment on the online version of the paper. Correspondence and requests for materials should be addressed to S.W. (Sabrina.wenzel@dlr.de).

Reviewer Information *Nature* thanks V. Brovkin and the other anonymous reviewer(s) for their contribution to the peer review of this work.

METHODS

Diagnosing the CO₂ fertilization factor. The long-term CO₂ fertilization factor is defined in this study as the fractional change over time of GPP in the biogeochemically coupled simulation experiment (referred to as 1%BGC). The CO₂ fertilization factor was diagnosed individually for all models for the Northern Hemispheric high latitudes (60° N–90° N) and the extratropics (30° N–90° N) for a doubling of atmospheric CO₂ concentration from its pre-industrial value of 285 p.p.m.v. Individual values for each model are listed in Extended Data Tables 1 and 2. As not all models provided output from year zero, the fractional change was calculated from five-year means centred on year 10 and year 70 and divided by a factor of 0.9 to account for the missing first 10% of the CO₂ increase.

Diagnosing the CO₂ effect on the CO₂ seasonal amplitude. The amplitude of the seasonal cycle is derived from the difference between the maximum and minimum monthly mean atmospheric CO₂ concentrations for each year. To estimate the effect of increasing atmospheric CO₂ concentrations ($\Delta C_A(t)$, where C_A is the atmospheric CO₂ concentration and t is time) on the CO₂ seasonal cycle amplitude ($\Delta C_{A,\text{ampl}}(t)$), we correlated these over the full length of the records available from the observations (see Methods section ‘Observational Data’) and the historical model simulations (1860–2005) for the CMIP5 models:

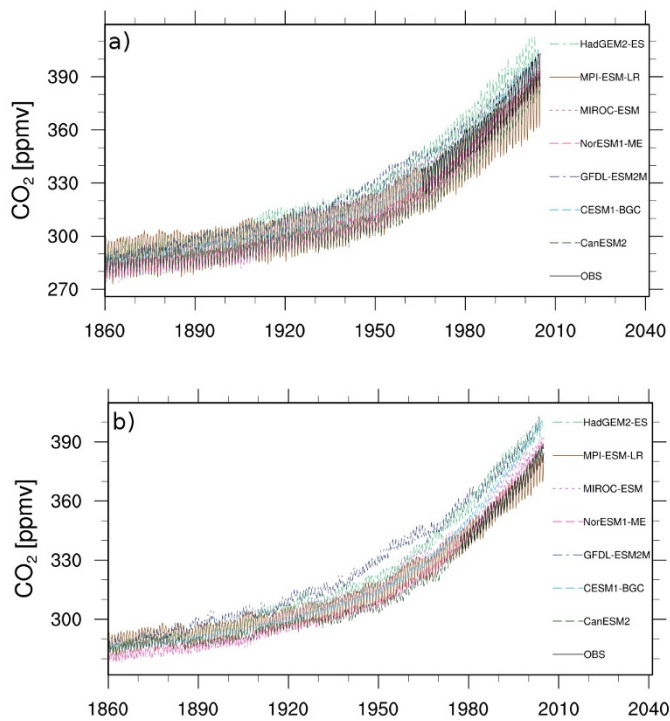
$$\Delta C_{A,\text{ampl}}(t) = a_0 + a \Delta C_A(t)$$

where a_0 and a are fitting parameters. Individual values for each model resulting from this equation are given in Extended Data Tables 1 and 2.

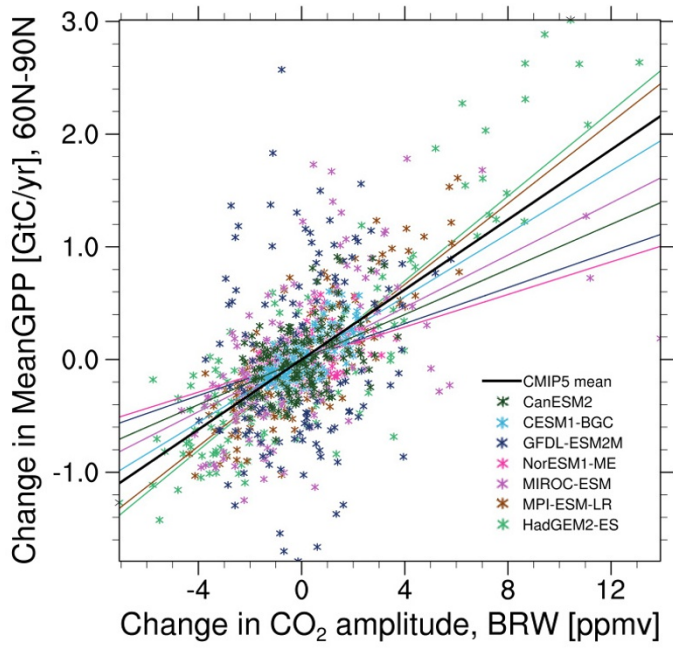
Observational Data. Observed monthly mean *in situ* atmospheric CO₂ concentrations at BRW (71.3° N, 156.6° W; record period 1974–2013) are from the National Oceanic and Atmospheric Administration (NOAA)/Earth System Research Laboratory (ESRL) (<http://www.esrl.noaa.gov/gmd/ccgg/trends>) and measurements at KMK (19.5° N, 155.6° W; record period 1979–present) from the Scripps Institute of Oceanography (http://www.scrippsco2.ucsd.edu/research/atmospheric_co2). Comparable data for the CMIP5 models were extracted as the near-surface CO₂ concentration for the closest grid box to each site.

Code availability. The routines used to reproduce this analysis from the CMIP5 model outputs are part of the ESMValTool¹⁹ and are available upon request from the corresponding author.

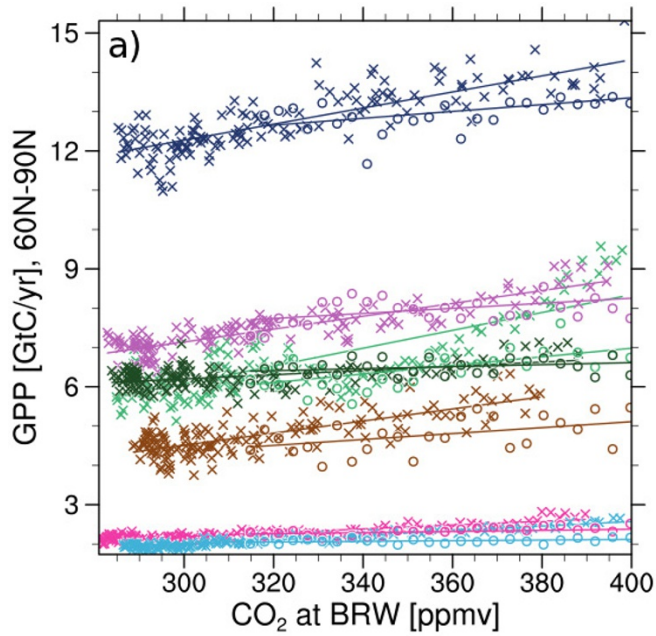
19. Eyring, V. *et al.* ESMValTool (v1.0) – a community diagnostic and performance metrics tool for routine evaluation of Earth system models in CMIP. *Geosci. Model Dev.* **9**, 1747–1802 (2016).



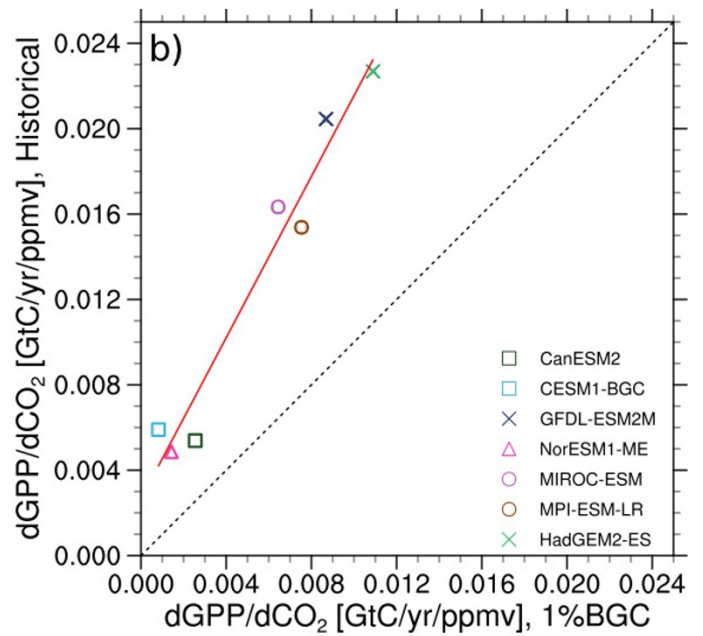
Extended Data Figure 1 | Simulated and observed CO₂ concentrations.
a, b, Time series of monthly mean atmospheric CO₂ between 1860 and 2005 at BRW (**a**) and KMK (**b**) at surface level, as simulated by the CMIP5 models in the historical simulations and observed (black lines) at each measuring site.



Extended Data Figure 2 | Annual mean high-latitude GPP (60° N–90° N) against the amplitude of the CO₂ seasonal cycle at BRW for each of the CMIP5 ESMs. The markers show the values for the individual years between 1850 and 2005 for the CMIP5 historical simulations and lines show the linear best fit for each model. The black line indicates the multi-model mean of the CMIP5 models.



Extended Data Figure 3 | Comparison of high-latitude GPP (60° N–90° N) versus annual mean CO₂. **a**, The correlation for both the historical (asterisks) and the 1%BGC (circles) CMIP5 model simulations. The markers show the values for the individual years and lines show the



linear best fit for each model. **b**, The comparison of the gradients in **a** for each model. The red solid line shows the gradient of the correlation and the black dashed line indicates a 1:1 correlation.

Extended Data Table 1 | Summary data for the changes in high-latitude GPP (60° N–90° N) and the amplitude of the CO₂ seasonal cycle at BRW

Model	GPP(2xCO ₂)/GPP(1xCO ₂)	Regression coefficients from linear regression	
		Offset to initial amplitude, a ₀ [ppmv]	CO ₂ sensitivity of amplitude, a [ppmv/ppmv]
CanESM2	1.18 ± 0.03	4.26 ± 1.10	0.020 ± 0.004
CESM1-BGC	1.22 ± 0.04	1.37 ± 1.26	0.023 ± 0.004
GFDL-ESM2M	1.25 ± 0.04	1.11 ± 1.62	0.027 ± 0.005
HadGEM2-ES	1.62 ± 0.11	-12.95 ± 1.53	0.108 ± 0.005
MIROC-ESM	1.38 ± 0.05	-2.36 ± 1.72	0.051 ± 0.005
MPI-ESM-LR	1.48 ± 0.12	2.18 ± 1.54	0.067 ± 0.005
NorESM1-ME	1.25 ± 0.04	2.86 ± 0.83	0.020 ± 0.003
OBS	-	-2.54 ± 2.49	0.050 ± 0.007

The fractional change in high-latitude GPP was calculated from the 1%BGC simulation for a doubling of CO₂ and is listed for each CMIP5 ESM. The regression coefficients result from a linear regression model for the change in the CO₂ amplitude at BRW (see Methods). Regressions are calculated using the full length of the records available from the CMIP5 historical simulations (1860–2005) and the BRW observations (1974–2013).

Extended Data Table 2 | Summary data for changes in extratropical GPP (30° N–90° N) and the amplitude of the CO₂ seasonal cycle at KMK

Model	GPP(2xCO ₂)/GPP(1xCO ₂)	Regression coefficients from linear regression	
		Offset to initial amplitude, a ₀ [ppmv]	CO ₂ sensitivity of amplitude, a [ppmv/ppmv]
CanESM2	1.33 ± 0.04	0.89 ± 0.63	0.010 ± 0.002
CESM1-BGC	1.26 ± 0.02	2.91 ± 0.31	0.000 ± 0.001
GFDL-ESM2M	1.44 ± 0.04	-1.07 ± 0.70	0.019 ± 0.002
HadGEM2-ES	1.59 ± 0.07	-6.65 ± 0.63	0.038 ± 0.002
MIROC-ESM	1.34 ± 0.04	-0.70 ± 0.57	0.019 ± 0.002
MPI-ESM-LR	1.56 ± 0.06	1.27 ± 0.90	0.031 ± 0.003
NorESM1-ME	1.21 ± 0.03	4.16 ± 0.35	-0.001 ± 0.001
OBS	-	4.84 ± 0.85	0.008 ± 0.002

The fractional change in extratropical GPP was calculated from the 1%BGC simulation for a doubling of CO₂ and is listed for each CMIP5 ESM. The regression coefficients result from a linear regression model for the change in the CO₂ amplitude at KMK (see Methods). Regressions are calculated using the full length of the records available from the CMIP5 historical simulations (1860–2005) and the KMK observations (1979–2015).